

Observations of Geomagnetic Induced Currents in Northwestern Russia: Case Studies

I. V. Despirak^{a,*}, P. V. Setsko^a, Ya. A. Sakharov^a, A. A. Lyubchich^a, V. N. Selivanov^b, and D. Valev^c

^a *Polar Geophysical Institute, Apatity, Murmansk oblast, Russia*

^b *Center for Physical and Technological Problems of Northern Energetics, Kola Science Center, Russian Academy of Sciences, Apatity, Murmansk oblast, Russia*

^c *Space Research and Technology Institute, Bulgarian Academy of Sciences, Stara Zagora, Bulgaria*

*e-mail: despirak@gmail.com

Received April 15, 2022; revised May 24, 2022; accepted May 25, 2022

Abstract—This paper analyzes a number of events of recorded intense geomagnetically induced currents (GICs) in transformers at stations located on the Karelia–Kola power transmission line in northwestern Russia and in a magnetometer at a gas pipeline compressor station located near the city of Mäntsälä in Finland. Located in the auroral and subauroral zones, these two different GIC recording systems made it possible to trace the occurrence and dynamics of GICs from subauroral to high latitudes and compare them with the motion of the substorm westward electrojet according to data obtained by the Scandinavian network of IMAGE magnetometers. For a detailed study, two events were considered (March 15, 2012 and March 17, 2013), when intense GICs were observed in the technological networks under consideration. It is shown that the development of GICs on the meridional observation profile is consistent with the latitudinal motion of the westward electrojet and corresponded to the appearance of successive substorm intensifications. In addition, a relationship has been established between the appearance of GICs and an increase in the intensity and wave activity of a substorm, determined from the IL and Wp geomagnetic indices.

DOI: 10.1134/S0016793222060032

1. INTRODUCTION

Rapid changes in the geomagnetic field are usually associated with the arrival of solar wind shock waves, coronal mass ejections (CMEs), and high-speed streams from coronal holes to the Earth, which lead to the development of magnetic storms and substorms, as well as the appearance of magnetic pulsations. These events are characterized by the induction of electric fields, which in turn can create intense low-frequency and quasi-direct currents in terrestrial technological networks, called geo-induced currents (GICs) (Lakhina et al., 2020; Pulkkinen et al., 2005; Viljanen et al., 2006). Thus, GICs are the final link in the Sun–solar wind–magnetosphere–ionosphere–Earth communication chain and can adversely affect power transmission lines, gas pipelines, telecommunications cables, and railway equipment up to their complete failure (Tsurutani et al., 2021). It should be noted that the GIC intensity depends on both the intensity of magnetic disturbances and the configuration of the technological system where these currents occur: the geographical location of the technological network, the Earth's surface conductivity at a given location, the technical condition of the network, etc. (Clilverd et al., 2018).

Along with studies of the causes of GICs, an important item of the protection from adverse effects of space weather is the monitoring geomagnetic field disturbances and recording of the development of GICs in actual power systems. The excitation of GICs in power transmission lines is controlled in many countries located in both high and middle geomagnetic latitudes, such as Finland, Great Britain, Canada, the United States, China, and Japan. Systems for protecting from the adverse impact of GICs as well as services for forecasting and warning about changes in geomagnetic activity are being developed. A number of Russian transformer substations of the Karelia–Kola power transmission line, which runs from south to north across Karelia and the Kola Peninsula, have a continuous metering system for GICs (Sakharov et al., 2019). The European Risk from Geomagnetically Induced Currents (EURISGIC) project organized a system of continuous observations at three to five nodes of the operating power transmission line from 2011 to the present (Sakharov et al., 2007, 2016). It should be noted that this GIC recording system is located at geographic latitudes from 60° to 69° N, where substorms are usually observed on a given meridian. The morphology of the development of geomagnetic disturbances in the auroral and subau-

ral zones allowed one to assume that the most significant source of GICs in northwestern Russia can be the intensification and motion of electrojets during the expanded phase of a substorm. In fact, it has been recently shown that the GIC intensity significantly increases with the growth of geomagnetic activity and peaks when the equatorial boundary of auroral oval precipitations is located by $\sim 1^\circ$ of latitude south of the GIC recording place (Vorobjev et al., 2018). In addition, the study of intense GICs (>30 A) over a 20-year period (1999–2019) at the Mäntsälä substation (located at a geographical latitude of $\sim 60.6^\circ$) in Finland revealed that the appearance of electrojets is most frequently (76%) associated with the amplification of auroral electrojets during supersubstorms ($SML < -2500$ nT) and intense substorms (-2500 nT $< SML < -2000$ nT) (Tsurutani et al., 2021).

This paper aims to analyze the relationship between the appearance of GICs and the spatio-temporal development of intense substorms. To do this, we used data from the GIC recording system in northwestern Russia and on the Mäntsälä gas pipeline in Finland. We considered the cases when the GIC at the Mäntsälä station exceeded 30 A and also at almost the same time a GIC was recorded on the Karelia–Kola power transmission line. In this paper, we consider two events that occurred on March 15, 2012 and March 17, 2013.

2. DATA

To analyze the appearance of GICs, we used data from two recording systems: data from the EURISGIC system (<http://eurisgic.ru>), which is located in the auroral zone of northwestern Russia, where the method of current recording in the neutral of a power transformer is used to measure the GIC (Sakharov et al., 2007, 2016) and data from the GIC detection system in Finland obtained for a gas pipeline near Mantsala (MAN) ($\sim 58^\circ$ MLAT) in the subauroral zone (<https://space.fmi.fi/gic/index.php>). Figure 1 shows the schematic of GIC recording substations and nearby observatories for measuring geomagnetic variations both in the North-West of Russia and in Finland. The arrows and inscriptions indicate the substations whose data are used in the work: Vykhodnoi (VKH) (68.8° N, 33.1° E), Revda (RVD) (67.9° N, 34.1° E), Kondopoga (KND) (62.2° N, 34.3° E), and Mantsala (MAN) (60.6° N, 25.2° E) stations; here, the geographical coordinates of the stations are indicated.

The spatial distribution of substorms was determined using magnetometers of the IMAGE (<http://space.fmi.fi/image>) and SuperMAG (<http://supermag.jhuapl.edu/>) networks. In addition, to study the spatial distribution of magnetic disturbances on the IMAGE profile, we analyzed the instant maps of the distribution of ionospheric equivalent electric currents (<https://space.fmi.fi/MIRACLE/>) (Viljanen and Häkkinen, 1997). It should be noted that these

maps are built in geographic coordinates, and, accordingly, we then indicate the geographic coordinates of magnetic observatories and GIC recording stations to compare the results. The global spatial distribution of substorms was also determined from the maps of magnetic field vectors obtained from observations on the SuperMAG network (Gjerloev, 2009; Newell and Gjerloev, 2011).

The local geomagnetic activity on the Scandinavian meridian of IMAGE was determined from the *IL*-index, which is calculated using the same technique as the *AL*-index (Davis and Sugiura, 1966), but from observations on the IMAGE network (https://space.fmi.fi/image/www/il_index_panel.php). In addition, the onset and development of substorms was controlled using the *Wp* (Wave and planetary) wave index, which characterizes the wave activity of a substorm, is associated with the power of Pi2 pulsations at low latitudes, and is calculated from data of 11 ground-based magnetic stations located between 20° and 50° MLAT around the North Pole (Nose et al., 2012) (<https://www.isee.nagoya-u.ac.jp/~nose.masahito/s-cubed/data/index.html>).

The development of auroras during a substorm was monitored using the MAIN (Multiscale Aurora Imaging Network) data obtained by an all-sky camera in Apatity (<http://aurora.pgia.ru>).

The conditions in the solar wind and the interplanetary magnetic field (IMF) before the onset of substorms were determined using the CDAWeb OMNI database (<http://cdaweb.gsfc.nasa.gov/>). The fluxes and structures of the solar wind were determined according to the catalog of large-scale solar wind phenomena (<ftp://ftp.iki.rssi.ru/omni/>) (Yermolaev et al. 2009).

3. RESULTS

3.1. The Event of March 15, 2012

The event of strong geomagnetic activity on March 7–17, 2012 can be attributed to the most disturbed periods of the ascending phase of solar cycle 24. This is a rather complicated case with four consecutive magnetic storms caused by different sources in the solar wind: by a coronal mass ejection (CME) and a high-speed stream (HSS), which followed but partially superimposed each other and overlapped. The development of storms and their sources in the solar wind have been analyzed in detail in several papers (Valchuk, 2013; Maris et al., 2014; Tsurutani et al. 2014). Figure 2 shows the parameters of the solar wind and the interplanetary magnetic field (IMF), from top to bottom: the magnitude (B_T) of the interplanetary magnetic field (IMF), the *Z*-component of the IMF (B_Z), the stream speed (V), the density, temperature, and dynamic pressure (P) of solar wind, and the geomagnetic indices *AL* and *SYM/H*. The left panel (Fig. 2a) shows the data for the time period covering all four



Fig. 1. A schematic of measuring instruments in the EURISGIC project: the circles denote the nearby observatories measuring the geomagnetic field and the GIC recording substations. The arrows and labels indicate the substations used in this study.

storms from March 6 to March 20, 2012; the right panel (Fig. 2b) shows the data for 1400 to 1900 UT on March 15, 2012. The boundaries of all magnetic storms are shown in Fig. 2a as vertical lines, denoted by S1, S2, S3, and S4, respectively. The S4 event began on March 15 at ~1230 UT, when the solar wind involves the first shock wave, which preceded the arrival of a CME composed of the region of compressed plasma (Sheath) and a magnetic cloud (MC). This CME was observed against the background of a high-speed solar wind stream (HSS) (Tsurutani et al., 2014). A strong southward IMF component (~ -15 nT) was recorded in the Sheath region, which led to the development of a magnetic storm (SYM/H = -80 nT). In addition, later, at ~1510 UT, a second shock wave was observed in the Sheath region, which caused small perturbations in the magnetic field variations at high-latitude stations and a burst of low-intensity GICs at Mäntsälä and Vykhodnoi stations (see Figs. 3 and 4 for details). Further, at the main phase of the magnetic storm at ~1700 UT, a local jump in the density and

dynamic pressure of the solar wind was observed. In our opinion, it is this jump in density that may be responsible for the development of an intense substorm in the auroral zone at around 1700 UT and the appearance of intense GICs ($>20-30$ A) at Mäntsälä and Vykhodnoi stations. In Figure 2, the observation times of substorms and GICs are shown as vertical dotted lines and labels (1) and (2).

Geomagnetic disturbances at 14–1800 UT on March 15, 2012 are shown in Fig. 3. The graphs in the upper panels (Fig. 3a) show the magnetograms of the X-component of the geomagnetic field at the Tartu–Ny-Ålesund (TAR-NAL) station chain of the IMAGE network. It can be seen that this time period had two substorm disturbances: at ~1500 and ~1700 UT, when the IMAGE chain was in the evening sector (~1800 and ~2000 LT). The first substorm was observed only at high latitudes; it began at ~1510 UT at the SOR station (70.5°N , 22.2°E) and then propagated to the NAL station (78.9°N , 11.9°E), where magnetic field variations of around -400 nT were observed. The sec-

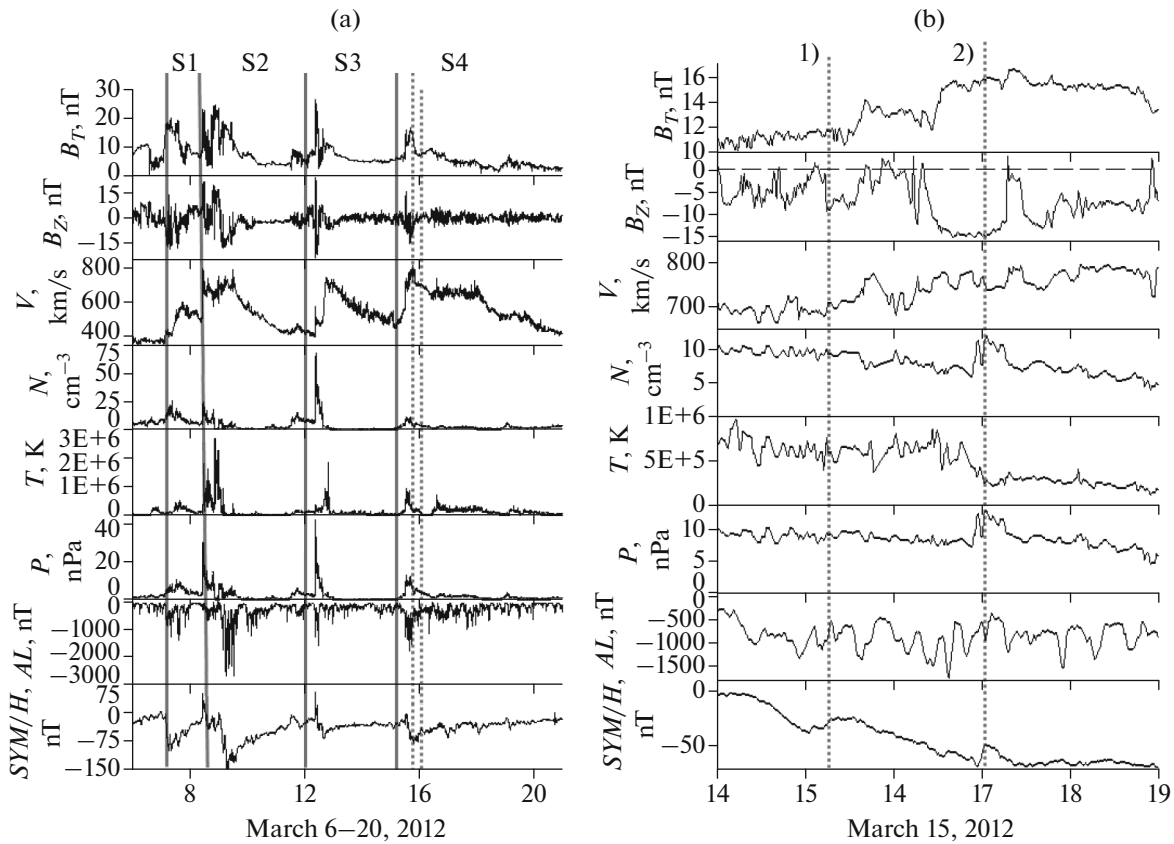


Fig. 2. The solar wind and IMF parameters, as well as geomagnetic indices for the time period (a) from 1200 UT March 7 to 0600 UT March 20, 2012 and (b) 1400–1900 UT March 15, 2012. From top to bottom: IMF magnitude (B_T), B_Z -component of the IMF (in the GSE system), stream velocity (V), density, temperature, and dynamic pressure of the solar wind (P), and geomagnetic indices AL and SYM/H . The boundaries of magnetic storms are denoted by vertical lines and labels S1, S2, S3, and S4. The onsets of substorms are marked as vertical dotted lines and labels (1) and (2).

ond substorm began at ~ 1655 UT at the HAN station (62.2° N, 26.6° E); the disturbances then propagated poleward, gradually appearing at higher latitudes: at SOR station (~ 1705 UT) and at NAL station (~ 1730 UT). Figure 3c (right panel) shows the maps of the spatial distribution of magnetic vectors obtained by the global SuperMAG system for 1530 and 1710 UT; magnetic vectors are rotated 90° clockwise to show the direction of ionospheric equivalent electric currents, midnight is at the bottom of the figure, and noon is at the top. According to spherical analysis of the map of SuperMAG magnetic field vectors at 1530 UT, a westward electrojet on the IMAGE meridian was observed in the evening sector (~ 1800 MLT) at geomagnetic latitudes above 70° MLAT, while an eastward electrojet was recorded at lower latitudes. While the second substorm at 1710 UT was characterized by a strong westwardly current over the Kola Peninsula and Spitsbergen, substorm disturbances were observed from subauroral to high latitudes.

Figure 3b shows the geomagnetic indices IL and Wp (top panels) and recorded GIC data for 1400 to 1800 UT on March 15, 2012, at the Mäntsälä, Kondo-

poga, Revda, and Vykhodnoi stations (bottom panels). The geomagnetic disturbances during the first substorm corresponded to small variations in the Wp index and actually were not reflected in the IL index. At the Mäntsälä station, small GICs with an intensity of ~ 5 A were observed at that time; however, the currents at the Vykhodnoi station were more significant (> 10 A). This may be associated with the fact that the first substorm was observed only at high latitudes. For the second substorm at ~ 1700 UT, sharp strong bursts are seen in IL (> -1000 nT) and Wp (> 2); then, at ~ 1710 and ~ 1720 UT, two minima in IL and one maximum in Wp were observed corresponding to the substorm propagation to high latitudes, which occurred in jumps (see Fig. 4 for details). The recorded GIC data at Mäntsälä, Kondopoga, Revda, and Vykhodnoi show that the onset of the second substorm at ~ 1700 UT coincides with the appearance of an intense GIC at Mäntsälä (~ 39 A). At the same time, induced currents appeared at Kondopoga (~ 7 A) and at Revda (~ 2 A) as well as rather intense GICs that began to appear at Vykhodnoi with maxima observed at ~ 1710 UT (~ 18 A),

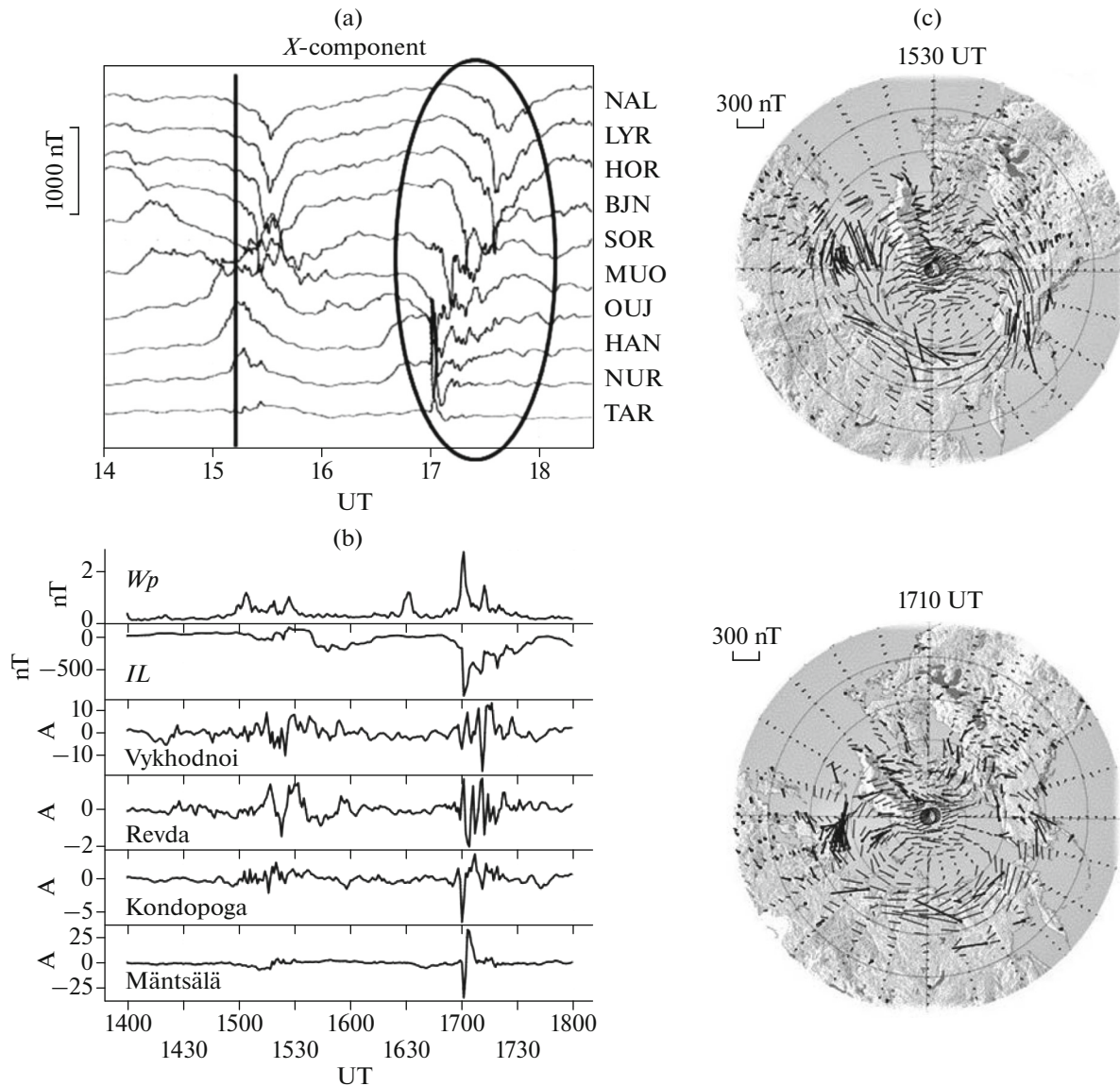


Fig. 3. Observations of geomagnetic disturbances and GIC records from 1400 to 1800 UT on March 15, 2012: (a) variations in the X -component of the magnetic field at IMAGE stations; (b) IL and W_p geomagnetic indices and GICs at Mäntsälä, Kondopoga, Revda, and Vykhodnoi stations; and (c) maps of the spatial distribution of magnetic field vectors obtained for the SuperMAG network. The magnetic vectors are rotated by 90° and indicate the direction of the equivalent electric currents. The maps were built for two times: 1530 and 1710 UT; noon and midnight are at the top and bottom, respectively; 0600 MLT (right) and 1800 MLT (left).

when the substorm westwardern electrojet reached the station latitude.

It should be noted that in the second substorm, the poleward movement of the westward electrojet was nonuniform, occurring in jumps, which can be clearly seen in Fig. 4, which shows the latitudinal profile of the westward and eastward electrojets calculated using the MIRACLE system from 1300 to 1900 UT on March 15, 2012. The westward electrojet is shown in dark gray and is denoted by “–” symbols and the eastward electrojet is shown in light gray and is denoted by “+” symbols. During the first substorm at ~ 1500 UT,

the westward electrojet developed only at 71° – 79° of geographical latitude. It follows from the bottom plots that significant GICs (>10 A) appeared only at Vykhodnoi station, which was close to the substorm onset latitude, while at substations located at lower latitudes (Mäntsälä, Kondopoga, and Revda), weak currents were observed (<5 A).

For the second substorm, it can be seen that at ~ 1700 UT the westward-electrojet started moving north of $\sim 60^\circ$ geographical latitude (HAN station), reached $\sim 69^\circ$ – 70° latitude at 17:10 UT (SOR), and then jumped to latitudes 74° – 78° (BJN–NAL). It

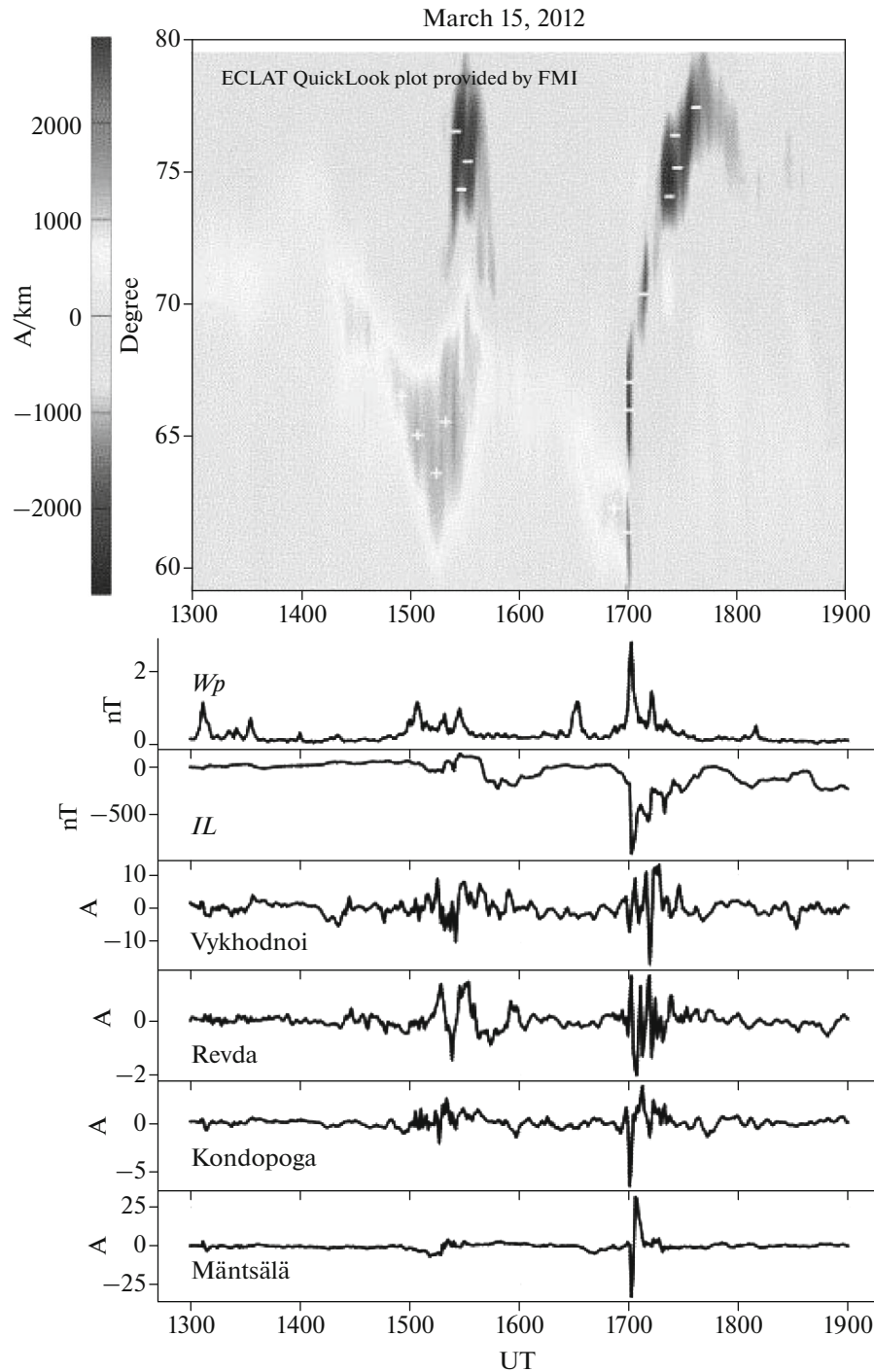


Fig. 4. The latitudinal profile of the development of westward and eastward electrojets, obtained using the MIRACLE system for 1300 to 1900 UT on March 15, 2012 (top). The westward electrojet is shown in dark gray with “-” symbols, and the eastward electrojet is shown in light gray with “+” symbols. Geomagnetic indices IL and W_p and the GICs at Mäntsälä, Kondopoga, Revda and Vykhodnoy stations from 1300 to 1900 UT on March 15, 2012 (bottom).

can be seen from the graphs on the bottom panel that the profiles of northward propagation of the GIC and westward electrojet almost coincide. An intense GIC appeared at the lowest latitude Mäntsälä substation simultaneously with the onset of the substorm at

1700 UT; small currents were also recorded in Kondopoga and Revda; at the Vykhodnoi substation, the maximum GIC occurred a little later than ~ 1710 UT, when a substorm westward electrojet appeared at the station latitude.

3.2. The Event of March 17, 2013

The second event of intense GICs on the Karelian-Kola power transmission line was recorded on March 17, 2013 (so-called St. Patrick's Day). That day was characterized by a moderate magnetic storm ($SYM/H = \sim -140$ nT) associated with the arrival of a CME to the Earth. Figure 5 shows the parameters of the solar wind and IMF for the time periods from 0000 UT on March 17 to 1200 UT on March 18 (Fig. 5a, left panel) and from 1200 to 2000 UT on March 17, 2013 (Fig. 5b, right panel). Figure 5 is similar to Fig. 2 except the graph of the AL -index. The magnetic cloud (MC) and the compressed plasma region (Sheath) are indicated by labels, and their boundaries by rectangles and a horizontal arrow. Two long periods of negative values of the IMF B_z component were observed in the CME: during Sheath and during MC. As a result, the magnetic storm developed as a typical two-stage storm (Kamide et al., 1998; Tsurutani et al., 1988). On March 17, three substorms were observed against the background of this magnetic storm. The times of appearance of these substorms and GIC recordings are shown by vertical dotted lines and labels 1, 2, and 3. It can be seen that all the three events occurred during the main phase of the storm and during the passage of the solar wind MC. Before their appearance, a long period of negative values of the IMF B_z component (~ -10 nT) was observed, the solar wind velocity was high (~ 600 km/s), and the density was also increased (~ 8 cm $^{-3}$).

The geomagnetic and auroral disturbances and induced currents (GICs) from 1500 to 2100 UT on March 17, 2013 are shown in Fig. 6. This figure is the same as Fig. 3 except for an additional graph showing the development of auroras, since observations by the all-sky camera were available at that time in Apatity (Fig. 6d). Figure 6a shows magnetograms of the X -component of the geomagnetic field at the chain of TAR–NAL stations of the IMAGE network. It can be seen that this time period involves three substorms: ~ 1550 , ~ 1800 , and ~ 1915 UT, when the IMAGE magnetometers were located in the evening sector (~ 1850 , ~ 2100 , and ~ 2215 MLT). The substorm times are indicated by ovals and labels 1, 2, and 3. The bottom plots show the geomagnetic indices IL and Wp and the GIC recording data (Fig. 6b); the left panel shows the SuperMAG maps of the spatial distribution of magnetic vectors for 1610, 1844, and 1930 UT, which are close to the times of maximum development of the substorms (Fig. 6c). The magnetic vectors on the maps are rotated by 90° and indicate the direction of the ionospheric equivalent electric currents. As follows from the first map at 1610 UT, the IMAGE chain was located in the evening sector ~ 1800 – 1900 MLT, where the Harang discontinuity is usually observed and currents of different directions (westward and eastward electrojets) are very close to each other (Harang, 1946; Despirak et al., 2021; Kunkel et al., 1986). It can be

seen that the westward electrojet at 1610 UT was located at latitudes of more than 67° – 68° geographic latitude; below, there was a rotation of magnetic vectors and an eastward current. According to the magnetograms, negative bays began at the PEL station and propagated to the NAL station; here, the strongest disturbances (~ 1000 nT) occurred at the SOR–BJN stations. At lower latitudes (OUJ–TAR), positive bays were observed. Comparing Figs. 6a and 6b, one can see that the appearance of GICs at the substations under consideration at approximately 1600 UT corresponds to the spatial location of the substorm westward electrojet: an intense current was observed at the Vykhodnoi substation (~ 27 A), where maximum magnetic field disturbances occurred; at lower latitudes, GICs appeared in Revda (~ 3 A), Kondopoga (~ 4 A), and Mäntsälä (~ 10 A).

The second substorm began at ~ 1800 UT at the NUR station and involved three activations at 1800, 1820, and 1840 UT, which are seen on the magnetograms as three negative bays (Fig. 6a) and as three minima (maxima) in $IL(Wp)$ indices (Fig. 6b). After the onset of the substorm, the electrojet moved poleward, the first three activations are seen at the NUR–OUJ stations; then, at ~ 1820 UT, disturbances appeared at the PEL–SOR stations. The second and third activations of the substorm are also clearly seen in the development of auroras (Fig. 6d), their times are marked by horizontal lines on the keogram of the all-sky camera in Apatity. It can be seen from Fig. 6b that the development of GICs at ~ 1800 – 1900 UT corresponds to the development of a substorm westward electrojet: at ~ 1800 UT, rather intense currents appeared at Mäntsälä and Kondopoga stations, while three GIC bursts with an intensity of ~ 32 A, 20 A, and 18 A were observed in Mäntsälä, corresponding to three activations of the substorm: at 1800, 1820, and 1840 UT, and two bursts with an intensity of ~ 10 and 11 A in Kondopoga, corresponding to the first and second activations of the substorm. At 1820 and 1840 UT, two GIC bursts with an intensity of ~ 3 A were recorded in Revda, corresponding to the second and third activations. At that time, the currents at the Vykhodnoi substation were insignificant, but later, at ~ 1930 UT, a rather intense induced current of ~ 27 A appeared. This time corresponds to the time of development of the third substorm. It follows from Fig. 6a that at ~ 1915 UT, disturbances began at the OUJ–SOR stations with an intensity of ~ -500 nT. At the time of the maximum development of the third substorm, strong GICs were recorded at the Vykhodnoi station. It should be noted that the third substorm was also recorded by the all-sky camera in Apatity (a breakup in auroras was fixed in Fig. 6d). The distributions of magnetic vectors of the SuperMAG network show that magnetic disturbances were observed just above the Kola Peninsula.

The movement of the westward electrojet during substorms is shown in more detail in Fig. 7, which gives the latitudinal profile of the westward and east-

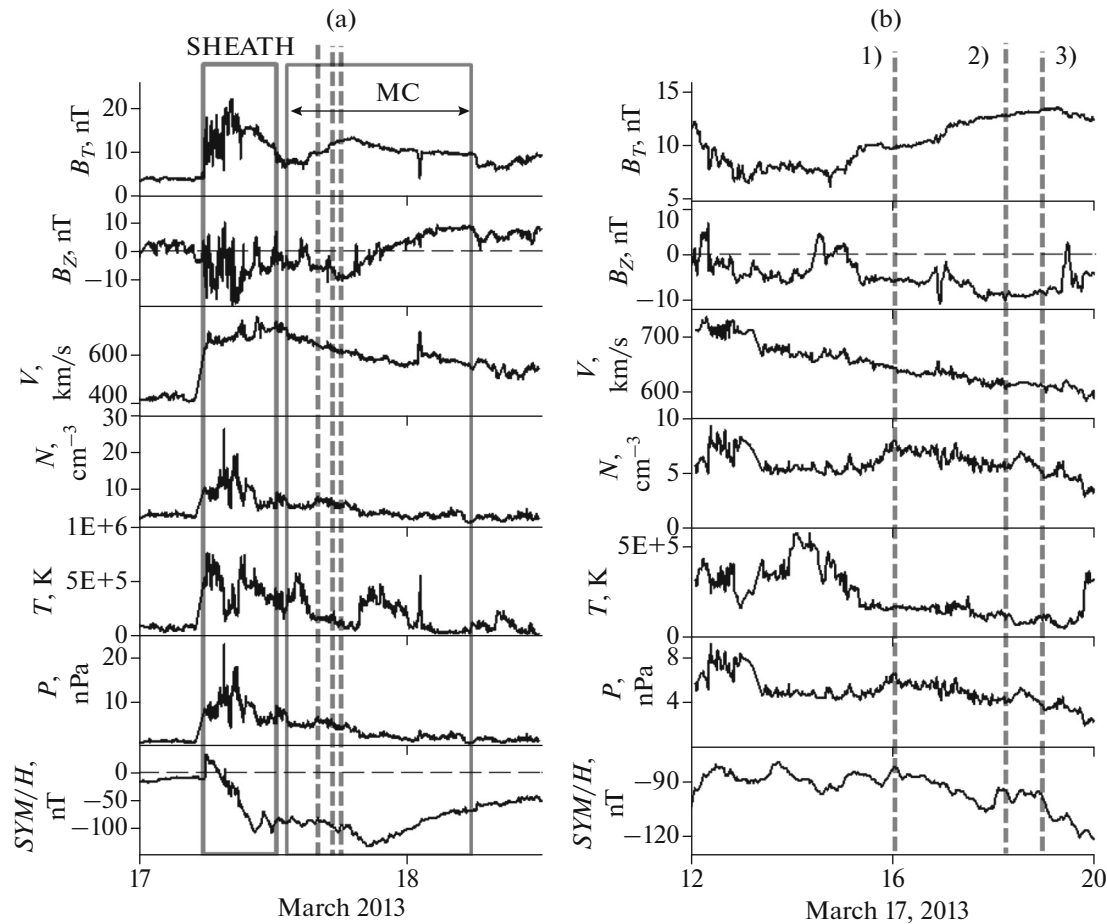


Fig. 5. The solar wind and IMF parameters as well as geomagnetic indices for (a) 0000 UT March 17 to 1200 UT March 18, 2013 and (b) 1200–2000 UT March 17, 2013. Figure 5 is the same as Fig. 2. The boundaries of the magnetic cloud (MC) and the SHEATH regions are indicated by rectangles and horizontal arrows; the onsets of substorms are marked by vertical dotted lines.

ward electrojets calculated by the MIRACLE system from 15 to 21 UT on March 17, 2013. Figure 7 is the same as Fig. 4. In the upper figure, the westward electrojet is marked in dark gray with symbols “—”; the geographic latitude is shown along the vertical axis. It can be seen that during the first substorm at ~1600 UT a rapid poleward movement of the westward electrojet was observed from ~68° to ~73° latitudes; the substorm then developed at latitudes of 73°–78°. Accordingly, intense GICs appeared at the Vykhodnoi and Revda substations during the movement of the electrojet to higher latitudes, while insignificant GICs were recorded at lower latitudes of the Kondopoga and Mäntsälä substations. The second substorm began at ~1800 UT at a latitude of ~60°; three substorm activations at 1800, 1820, and 1840 UT are clearly seen on the latitudinal profile. During the first two activations, the westward electrojet was observed at latitudes of 60°–65°, while during the third activation, the electrojet advanced to the pole up to ~71°. Then, at 1915 UT, the third substorm began developing at latitudes of 66°–69°. It can be seen from the lower graphs

that the GIC development was similar to the spatio-temporal dynamics of the westward electrojet. At ~1600 UT, intense GICs were observed at Revda and Vykhodnoi stations; during the second substorm, all three electrojet activations were reflected in the GIC at Mäntsälä station, the first two activations were reflected at the Kondopoga station, and the second and third activations were reflected at Revda. At the Vykhodnoi station, the GIC appeared during the third substorm.

4. DISCUSSION

We analyzed two events of intense GICs observed on different recording systems: the Karelia–Kola system in northwestern Russia and the Finnish gas pipeline near Mäntsälä. Both events were observed during magnetic storms caused by the arrival of interplanetary coronal mass ejections (ICMEs) to the Earth. It should be noted that the appearance of GICs at substations in northwestern Russia has been studied since 2011 and it was found that intense GICs are mainly

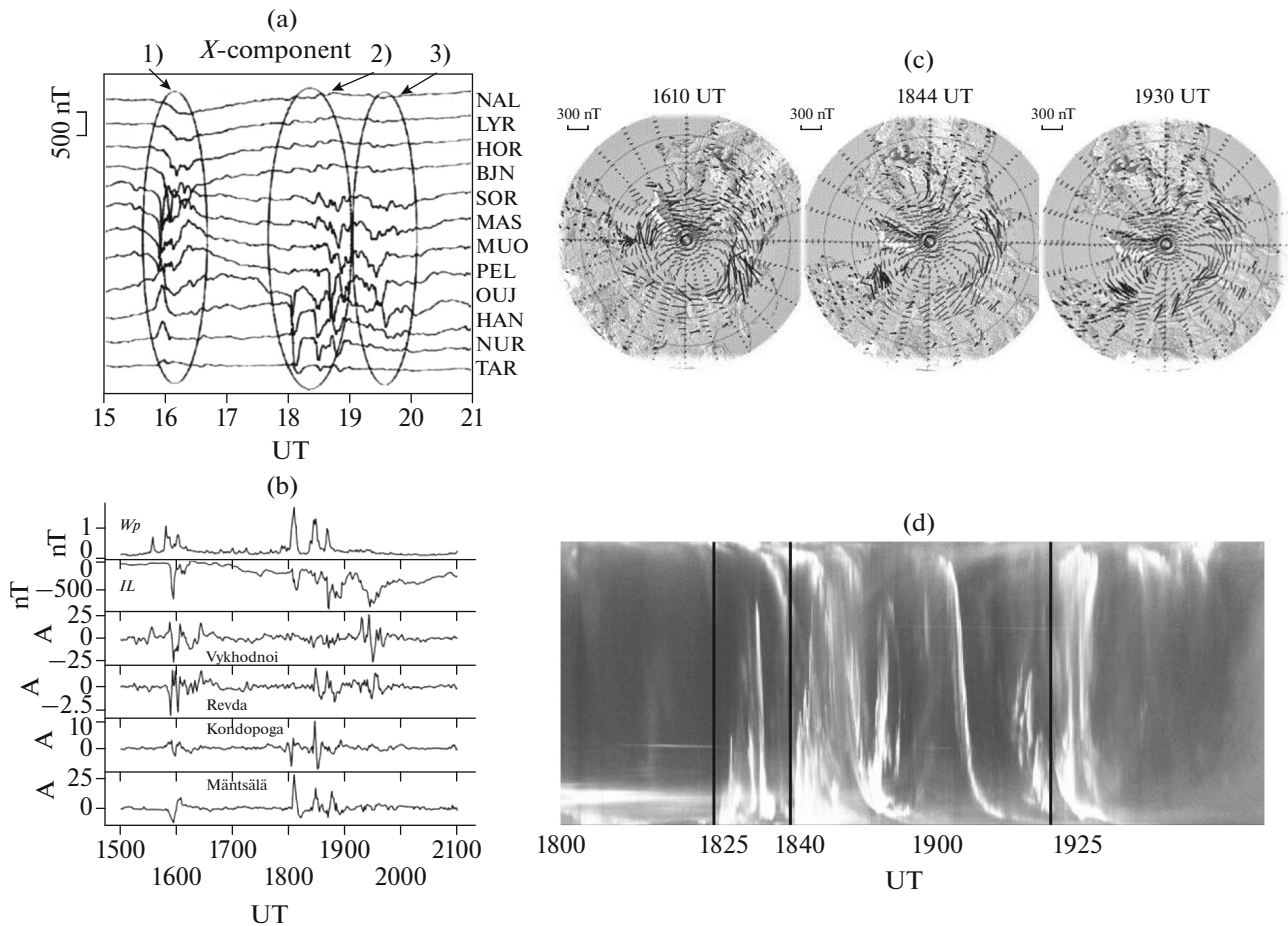


Fig. 6. Observed geomagnetic disturbances and recorded GICs from 1500 to 2100 UT on March 17, 2013. (a) Variations in the X-component of the magnetic field at IMAGE stations. (b) Geomagnetic indices IL and W_p and GICs at Mäntsälä, Kondopoga, Revda, and Vykhodnoi stations. (c) Maps of the spatial distribution of magnetic field vectors, obtained for the SuperMAG network for 1610, 1844, and 1930 UT (magnetic vectors are rotated by 90° and indicate the direction of equivalent electric currents). (d) Aurora keogram in Apatity from 1800 to 2000 UT; vertical lines indicate the times of substorm activations.

associated with CMEs (Sakharov et al., 2019). The same result was also obtained for GICs recorded on the Mäntsälä gas pipeline: 91% of days with GIC peaks greater than 10 A are associated with ICMEs (Huttunen et al., 2008). Analysis of a large time interval (from 1999 to 2019) indicated that among different types of solar wind, ICMEs are responsible for $\sim 97\%$ of GIC > 10 A peaks, while $\sim 51\%$ and $\sim 44\%$ of all peaks are associated with Sheath and MC, respectively (Haira, 2022; Tsurutani et al., 2021). It is known that the occurrence of very intense magnetic storms is associated with the arrival of ICMEs (Echer et al., 2008); consequently, most GICs can also be observed during intense storms. It turned out that $\sim 67\%$ of all GIC > 10 A peaks at Mäntsälä station were observed during superstorms ($SYM/H > -250$ nT); in this case, the vast majority of them occurred during the main phase of the storm (Haira, 2022). Both intense GICs considered in our study were also recorded during the

main phases of the magnetic storms on March 15, 2012 and March 17, 2013 (Figs. 2 and 5).

In addition, it is known that other, more local, disturbances of the magnetic field associated with magnetospheric substorms, impulses of the solar wind dynamic pressure, magnetic pulsations, omega structures in auroras, etc., can also affect the occurrence of GICs (Apatenkov et al., 2019; Kozyreva et al., 2020; Oliveira et al., 2017; Vorobjev et al., 2019). An important source of GICs in the auroral zone is the intensification and motion of electrojets during the expansion phase of a substorm. In this study, we used data from two different GIC recording systems, which allowed us to trace their dynamics from subauroral to high latitudes (from 60.6° N to 69° N of geographic latitude) and compare them with the latitudinal development of the substorm. It can be seen from Figs. 3–4 and Figs. 6 and 7 that the appearance of GICs at substations located at different latitudes is similar to the latitudinal profile of a westward electrojet. When the substorm developed

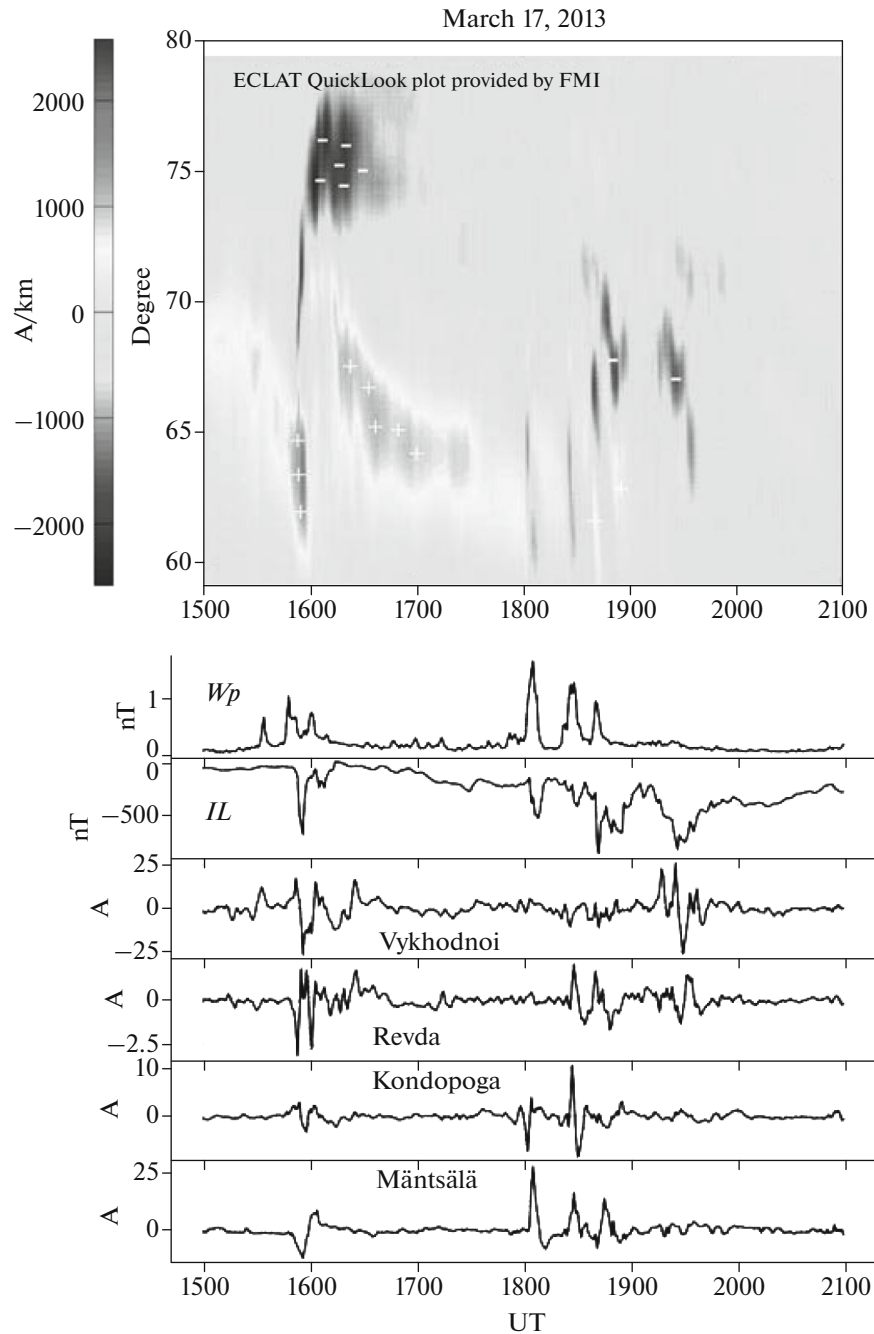


Fig. 7. Latitudinal profile of the development of westward and eastward electrojets, obtained using the MIRACLE system, for 1500 to 2100 UT on March 17, 2013 (top). Geomagnetic indices IL and W_p as well as GICs at Mäntsälä, Kondopoga, Revda, and Vykhodnoi stations (bottom). Fig. 7 is the same as Fig. 4.

only at high latitudes (at ~ 1530 UT on March 15, 2012 and at ~ 1600 UT on March 17, 2013), GICs appeared only at the high-latitude Revda and Vykhodnoi substations. For the substorm that occurred at ~ 1700 UT on March 15, 2012, the electrojet moved along the entire latitudinal profile from subauroral to high latitudes and, accordingly, GICs appeared at all substations starting from Mäntsälä and gradually propagating to higher latitude stations with some time delay

(Fig. 4). The most striking similarity in the latitudinal profile of the appearance of GICs and the development of the westward electrojet was manifested for the substorm on March 17, 2013 at ~ 1800 UT. This was a complex event consisting of three substorm activations, when geomagnetic disturbances started at Mäntsälä and propagated to higher latitudes (Fig. 6). This fine spatio-temporal structure of the substorm manifested itself in the development of GICs: all three

activations appeared as three GIC peaks (~32 A, 20 A, and 18 A) at Mäntsälä; then, the first and second activations are seen as GIC peaks at Kondopoga (~10 A and 11 A) and the second and third activation as GIC peaks (~3 A) at Revda. A little later, a GIC (~27 A) appeared at Vykhodno (Figs. 6 and 7). We believe that the study and modeling of GIC sources should also take into consideration the fact that the substorm activity is not only associated with an increase in the intensity of a large-scale azimuthal westward electrojet (Belakhovsky et al., 2018), but also has other smaller scale meridional manifestations, such as the poleward motion of the westward electrojet (Kisabeth and Rostoker, 1974; Pudovkin et al., 1995), which occurs in “jumps” during the expansion phase of a substorm (Wiens and Rostoker, 1975). In addition, the expansion phase of a substorm can involve several activations (Sergeev and Yahnin, 1979), as was observed during the substorm that occurred at ~1800 UT on March 17, 2013.

Both events under consideration (March 15, 2012 and March 17, 2013) are also characterized by a good correlation between the appearance of GICs and the *IL* index, which characterizes the intensity of the westward electrojet at the IMAGE stations (by analogy with the *AL* index). It should be noted that the March 17, 2013 event was previously considered in (Belakhovsky et al., 2018, 2019). However, the authors did not find a correlation between GICs and the *AE* index, possibly because they used the hourly values of *AE*, which is insufficient in the case of substorms and fails to reveal their fine structure. In addition, in the case of such a complex event as the 1800 UT substorm on March 17, 2013, the *IL* index, which reflects disturbances exactly on the IMAGE meridian, is better suited, since it allows the influence of substorm activity at other longitudes to be excluded.

We also revealed a good correlation between the occurrence of GICs and the *Wp* index, which can be used as an indicator of the substorm onset (Nose et al., 2012) (Figs. 3–4, 6 and 7). However, it should be noted that this dependence is well traced for the Mäntsälä and Kondopoga stations but may not manifest itself at the Revda and Vykhodnoi stations, as for the case of the substorm that occurred at ~1930 UT on March 17, 2013. In our opinion, this happens because the *Wp*-index is calculated with respect to low-latitude stations, and disturbances at higher latitudes may not be reflected in its variations (Figs. 6 and 7).

5. CONCLUSIONS

(1) The development of GICs on the meridional profile (from Mäntsälä to Vykhodnoi) occurred in accordance with the fine spatio-temporal structure of the substorm. The appearance of GICs at different latitudes is similar to the poleward movement of the westward electrojet and the appearance and poleward propagation of substorm activations.

(2) A relationship has been established between the appearance of GICs and an increase in the geomagnetic indices: *IL*, characterizing the intensity of the westward electrojet on the IMAGE meridian and *Wp*, which determines the onset and wave activity of a substorm.

ACKNOWLEDGMENTS

The authors are grateful to the creators of the OMNI database (<http://omniweb.gsfc.nasa.gov>), the catalog of large-scale solar-wind types (<ftp://ftp.iki.rssi.ru/pub/omni/catalog>), the SuperMAG database (<http://supermag.jhuapl.edu/>), and IMAGE (<http://space.fmi.fi/image/>) for the permission to use these data in the study.

FUNDING

The work by I.V. Despirak, A.A. Lyubchich, and P.V. Setsko was supported by the Russian Foundation for Basic Research and the National Science Foundation of Bulgaria, project no. 20-55-18003. The work by D. Valev was supported by the National Science Foundation of Bulgaria, project no. KP-06-Rusiya/15. The work by Ya.A. Sakharov and V.N. Selivanov was supported by the Russian Science Foundation, project no. 22-29-00413.

CONFLICT OF INTEREST

The authors declare that they have no conflicts of interest.

REFERENCES

- Belakhovsky, V.B., Pilipenko, V.A., Sakharov, Ya.A., and Selivanov, V.N., Characteristics of the variability of a geomagnetic field for studying the impact of the magnetic storms and substorms on electrical energy systems, *Izv., Phys. Solid Earth*, 2018, no. 1, pp. 52–65.
- Belakhovsky, V., Pilipenko, V., Engebretson, M., Sakharov, Y., and Selivanov, V., Impulsive disturbances of the geomagnetic field as a cause of induced currents of electric power lines, *J. Space Weather Clim.*, 2019, vol. 9, p. A18. <https://doi.org/10.1051/swsc/2019015>
- Clilverd, M.A., Rodger, C.J., Brundell, J.B., Dalzell, M., Martin, I., Macmanus, D.H., Thomson, N.R., Petersen, T., and Obana, Y., Long-lasting geomagnetically induced currents and harmonic distortion observed in New Zealand during the 7–8 September 2017 disturbed period, *Space Weather*, 2018, vol. 16, pp. 704–717. <https://doi.org/10.1029/2018SW001822>
- Davis, T.N. and Sugiura, M., Auroral electrojet activity index AE and its universal time variations, *J. Geophys. Res.*, 1966, vol. 71, pp. 785–801. <https://doi.org/10.1029/JZ071i003p00785>
- Despirak, I.V., Kozelova, T.V., Kozelov, B.V., and Lyubchich, A.A., Observations of substorm activity from the data of main camera system and THD satellite in the plasma sheet, in *Proceedings of 44th Annual Seminar*

- “*Physics of Auroral Phenomena*”, Apatity, 2021, pp. 16–19.
<https://doi.org/10.51981/2588-0039.2021.44.003>.
- Echer, E., Gonzalez, W.D., and Tsurutani, B.T., Interplanetary conditions leading to superintense geomagnetic storms ($Dst \leq -250$ nT) during solar cycle 23, *Geophys. Res. Lett.*, 2008, vol. 35, p. L06S03.
<https://doi.org/10.1029/2007GL031755>
- Gjerloev, J.W., A global ground-based magnetometer initiative, *Eos Trans. Am. Geophys. Union*, 2009, vol. 90, pp. 230–231.
<https://doi.org/10.1029/2009EO270002>
- Haira, R., Intense geomagnetically induced currents (GICs): Association with solar and geomagnetic activities, *Sol. Phys.*, 2022, vol. 297, p. 14.
<https://doi.org/10.1007/s11207-021-01945-8>
- Harang, L., The mean field of disturbance of polar geomagnetic storms, *Terr. Magn. Atmos. Electr.*, 1946, vol. 51, no. 3, pp. 353–380.
<https://doi.org/10.1029/TE051i003p00353>
- Huttunen, K.E.J., Kilpua, S.P., Pulkkinen, A., Viljanen, A., and Tanskanen, E., Solar wind drivers of large geomagnetically induced currents during the solar cycle 23, *Space Weather*, 2008, vol. 6, no. 10, S10002.
<https://doi.org/10.1029/2007SW000374>
- Kamide, Y., Yokoyama, N., Gonzalez, W., Tsurutani, B.T., Daglis, I.A., Brekke, A., and Masuda, S., Two-step development of geomagnetic storms, *J. Geophys. Res.*, 1998, vol. 103, pp. 6917–6921.
<https://doi.org/10.1029/97JA03337>
- Kisabeth, J.L. and Rostoker, G., The expansive phase of magnetospheric substorms. I. Development of the auroral electrojets and auroral arcs configuration during substorm, *J. Geophys. Res.*, 1974, vol. 79, pp. 972–984.
<https://doi.org/10.1029/JA079i007p00972>
- Kozyreva, O., Pilipenko, V., Krasnoperov, R., Baddeley, L., Sakharov, Y., and Dobrovolsky, M., Fine structure of substorm and geomagnetically induced currents, *Ann. Geophys.*, 2020, vol. 63, no. 2, p. GM219.
<https://doi.org/10.4401/ag-8198>
- Kunkel, T., Untiedt, J., Baumjohann, W., and Greenwald, R., Electric fields and currents at the Harang discontinuity: A case study, *J. Geophys.*, 1986, vol. 59, no. 1, pp. 73–86.
- Lakhina, G.S., Hajra, R., and Tsurutani, B.T., Geomagnetically induced current, in *Encyclopedia of Solid Earth Geophysics*, Gupta, H.K., Ed., Springer Nature Switzerland AG, 2020.
https://doi.org/10.1007/978-3-030-10475-7_245-1
- Maris Muntean, G., Besliu-Ionescu, D., Georgieva, K., and Kirov, B., Analysis of the geomagnetic activity during the SC 24 maximum phase, in *6th Workshop “Solar Influences on the Magnetosphere, Ionosphere and Atmosphere”, 26–30 May 2014, Sunny Beach, Bulgaria, Abstracts Book*, 2014, p. 10. <http://ws-sozopol.stil.bas.bg/>.
- Newell, P.T. and Gjerloev, J.W., Substorm and magnetosphere characteristic scales inferred from SuperMAG auroral electrojet indices, *J. Geophys. Res.*, 2011, vol. 116, p. A12211.
<https://doi.org/10.1029/2011JA016936>
- Nosé, M., Iyemori, T., Wang, L., et al., Wp index: A new substorm index derived from high-resolution geomagnetic field data at low latitude, *Space Weather*, 2012, vol. 10, no. 8, p. 08002.
<https://doi.org/10.1029/2012SW000785>
- Oliveira, D.M. and Ngwira, C.M., Geomagnetically induced currents: Principles, *Braz. J. Phys.*, 2017, vol. 47, pp. 552–560.
<https://doi.org/10.1007/s13538-017-0523-y>
- Pudovkin, M.I., Semenov, V.S., Kotikov, A.L., and Shishkina, E.M., Dynamics of auroral electrojets and energetics of substorm, *J. Atmos. Terr. Phys.*, 1995, pp. 187–192.
[https://doi.org/10.1016/0021-9169\(93\)E0033-6](https://doi.org/10.1016/0021-9169(93)E0033-6)
- Pulkkinen, A., Lindahl, S., Viljanen, A., and Pirjola, R., Geomagnetic storm of 29–31 October 2003: Geomagnetically induced currents and their relation to problems in the Swedish high-voltage power transmission system, *Space Weather*, 2005, vol. 3, no. 8, p. C08C03.
<https://doi.org/10.1029/2004SW000123>
- Sakharov, Ya.A., Danilin, A.N., and Ostafiichuk, R.M., Recording of GICs in power systems of the Kola Peninsula, in *Trudy 7-go Mezhdunar. simp. po elektromagnitnoi sovmestimosti i elektromagnitnoi ekologii* (Proceedings of the 7th International Symposium on Electromagnetic Compatibility and Electromagnetic Ecology), St. Petersburg: IEEE, 2007, pp. 291–293.
- Sakharov, Ya.A., Kat’kalov, Yu.V., Selivanov, V.N., and Viljanen, A., Recording of GICs in a regional power system, in *Prakticheskie aspekty geliogeofiziki, Materialy spetsial’noi sekcii “Prakticheskie aspekty nauki kosmicheskoi pogody” 11-i ezhegodnoi konferentsii “Fizika plazmy v solnechnoi sisteme”* (Practical Aspects of Helio-geophysics: Proceedings of the Special Section “Practical Aspects of the Science of Space Weather” of the 11th Annual Conference “Physics of Plasma in the Solar System”), Moscow: IKI, 2016, pp. 134–145.
- Sakharov, Ya.A., Selivanov, V.N., Bilin, V.A., and Nikolaev, V.G., Extreme values of GICs in a regional power system, in *Proc. XLII Annual Seminar “Physics of Auroral Phenomena”*, Apatity, 2019, pp. 53–56.
<https://doi.org/10.25702/KSC.2588-0039.2019.42.53-56>
- Sergeev, V.A. and Yahnin, A.G., Correspondence of the substorm explosive phase signatures, in *Geomagnitnye issledovaniya* (Geomagnetic Investigations), Moscow: Sov. Radio, 1979, vol. 24, pp. 78–89.
- Tsurutani, B.T. and Hajra, R., The interplanetary and magnetospheric causes of geomagnetically induced currents (GICs) > 10 Å in the Mäntsälä Finland pipeline: 1999 through 2019, *J. Space Weather Clim.*, 2021, vol. 11, p. A23.
<https://doi.org/10.1051/swsc/2021001>
- Tsurutani, B.T., Gonzalez, W.D., Tang, F., Akasofu, S.-I., and Smith, E.J., Solar wind southward B_z features responsible for major magnetic storms of 1978–1979, *J. Geophys. Res.*, 1988, vol. 93, no. A8, pp. 8519–8531.
<https://doi.org/10.1029/JA093iA08p08519>

- Tsurutani, B.T., Echer, E., Shibata, K., Verkhoglyadova, O.P., Mannucci, A.J., Gonzalez, W.D., Kozyra, J.U., and Pätzold, M., The interplanetary causes of geomagnetic activity during the 7–17 march 2012 interval: A CAUSES II overview, *J. Space Weather Space Clim.*, 2014, vol. 4, p. A02.
<https://doi.org/10.1051/swsc/2013056>
- Val'chuk, T.E., The solar wind and magnetic storms of cycle 24 of solar activity, *Astron. Tsirk.*, 2013, no. 1585.
- Viljanen, A. and Häkkinen, L., IMAGE magnetometer network, in *Satellite – Ground Based Coordination Sourcebook*, Lockwood, M., Wild, M.N., and Opgenoorth, H.J., Eds., Noordwijk, The Netherlands: ESA, 1997, pp. 111–117.
- Viljanen, A., Tanskanen, E.I., and Pulkkinen, A., Relation between substorm characteristics and rapid temporal variations of the ground magnetic field, *Ann. Geophys.*, 2006, vol. 24, no. 2, pp. 725–733.
<https://doi.org/10.5194/angeo-24-725-2006>
- Vorob'jev, A.V., Pilipenko, V.A., Sakharov, Ya.A., and Selivanov, V.N., Statistical relationships between variations of the geomagnetic field, auroral electrojet, and geomagnetically induced current, *J. Sol.-Terr. Phys.*, 2019, vol. 5, no. 1, pp. 35–42.
<https://doi.org/10.12737/stp-51201905>
- Vorob'jev, V.G., Sakharov, Ya.A., Yagodkina, O.I., Petrukovich, A.A., and Selivanov, V.N., Geoinduced currents and their relationship with the western electrojet position and auroral precipitation boundaries, *Tr. Kol'sk. Nauchn. Tsentra Ross. Akad. Nauk*, 2018, vol. 4, pp. 16–28.
<https://doi.org/10.25702/KSC.2307-5252.2018.9.5.16-28>
- Wiens, R.G. and Rostoker, G., Characteristics of the development of the westward electrojet during the expansive phase of magnetospheric substorms, *J. Geophys. Res.*, 1975, vol. 16, pp. 2109–2128.
<https://doi.org/10.1029/JA080i016p02109>
- Yermolaev, Yu.I., Nikolaeva, N.S., Lodkina, I.G., Yermolaev, M.Yu., Catalog of large-scale solar wind phenomena during 1976–2000, *Cosmic Res.*, 2009, vol. 47, no. 2, pp. 81–94.

Translated by V. Arutyunyan